View metadata, citation and similar papers at core.ac.uk

brought to you by CORE

provided by Illinois Digital Environment for Access to Learning and Scholarship Repository

© 2017 Moongee Cho

# COIL ANTENNA DESIGN FOR TRANSMITTER AND RECEIVER FOR BIOELECTRONICS

BY

MOONGEE CHO

THESIS

Submitted in partial fulfillment of the requirements
for the degree of Master of Science in Electrical and Computer Engineering
in the Graduate College of the
University of Illinois at Urbana-Champaign, 2017

Urbana, Illinois

Advisor:

Professor John A. Rogers

# ABSTRACT

Bioelectronics, which record the electrical activity of organisms, have become one of the major research areas for many purposes. Effectively adaptable and minuscule electronics led to this new era of bio-signal recording. Biomedical electronics also have soft and flexible characteristics with skin-mountable applications. Since bioelectronics are small enough to be portable, they allow the operation of devices without any limitations incurred by wired communications. Therefore, portable and skin-mountable devices require wireless power transfer between the devices and the transmitter. The wireless sensor network based on a near-field communication (NFC) increases the capability of the devices with a great power efficiency. This thesis shows an inductive link of the coil antenna designs that present a wireless power transfer system based on a near-field communication. The coil antennas contribute the electronics to receive power wirelessly and monitor the collected data continuously. Both coil antennas for the transmitter and the receiver are constructed of a material based on the conductivity with cost-effectiveness. In addition, the receiving antenna is designed based on soft and flexible materials so that it can be attached to the skin with bioelectronics.

# ACKNOWLEDGMENTS

I would like to thank my research advisor, Professor John A. Rogers, for supporting my research throughout my undergraduate and graduate degrees. He has given me wonderful opportunities to develop my knowledge through the passion and great vision of his teaching. I would like to thank my academic advisor Professor Erhan Kudeki. He inspired my interest in my current specialization area and supported me to join my current research group. In addition, I would like to thank my research mentor Ha Uk Chung for helping my contribution in many different research projects. Also, I would like to thank Jungho Yi, Jong Yoon Lee, and Jaeseok Jeong for assisting me. Finally, I would like to thank my family for always supporting me.

TABLE OF CONTENTS

# CHAPTER 1: INTRODUCTION

The physiological signals on the human skin have attracted much interest of many researchers starting in 1929 [1]. In a bioelectronic system, often called epidermal electronics, a device can be attached to the human skin and monitor bio-signals continuously [2]. This new system brought bioelectronics that have not only multiple functionalities, but also soft and flexible. This bioelectronic system also allows the implementation with various target applications such as implantable optogenetics [3], [4]. However, the use of epidermal electronics has limitations attributed by power supply systems. If the electronics are powered directly from batteries or other power sources connected with wires, there is no way to operate the electronics at the places that do not have power outputs. Since the functionality of devices should not be limited by the wires, the wireless communication, including the wireless power transfer, offers a considerable improvement of the portability of the skin-mountable devices [1]. Therefore, the wireless power transfer system based on the near-field communication is necessary for efficient uses of biomedical electronics.

Wireless sensor networks and near-field communication systems have attracted the interest of many researchers in recent years [5]. In all these systems, most communication links are either determined by far-field wideband antennas or a near-field communication (NFC) link [6], [7]. Since the near-field communication

link is operated by a near-field antenna or inductive coils, the wireless power transfer is important to be considered. In a usual inductive link, the transmitter circuit provides a low impedance load to the source before the primary coil, and the receiver circuit is in parallel resonance at a resonant frequency to get improved power at the load [5].

In order to design an inductive coil link for a near-field communication system, an antenna for a transmitter should deliver as much power necessary to an antenna for a receiver. There are three considerations to design coil antennas of a transmitter and a receiver for bioelectronic applications: (1) right combinations of materials to allow the bioelectronics to be soft and flexible, (2) patternable designs with proper dimensions and sizes, and (3) a wireless operation in radiofrequency (RF) bands that minimize the signal reflection and interference [3]. The material for antennas should provide conductivity with a reasonable cost to prevent energy loss at the antennas [9]. Moreover, the materials that covers the bioelectronic power transferring system, especially the receiver system, are selected based on their bio-compatibilities, low modulus, elastic mechanical properties, and compatibilities with simple processes of the fabrication [8]. The size and dimension of selected antennas for the transmitter and the receiver depend on the power efficiency [5]. The antenna for the transmitter delivers the power with less return loss and the antenna for the receiver accepts as much of the power as possible at the near-field communication operating frequency of 13.56 MHz.

In this thesis, the antenna designs for a transmitter and a receiver are introduced and optimized by various simulations and measurements. In addition, the actuation system is presented as a bioelectronic application of the wireless power transfer system. The actuation system, which consists of several actuation sensors and accepts sensors to be operated independently, is composed of soft, flexible, and stretchable materials so that the system can be attached to the skin without the occurrence of damage.

# CHAPTER 2: TRANSMITTER ANTENNA CIRCUIT DESIGN

Chapter 2 introduces theoretical requirements of a coil antenna design for a transmitter to deliver the power to a receiver wirelessly. An impedance matching method for an antenna for a transmitter to transfer power without unexpected power loss is introduced.

## 2.1. Theoretical Requirements

### 2.1.1. Antenna Design Considerations

There are several considerations to design a rectangular coil antenna for the transmitter with a radiation of an expected power. The input radiated power of a coil antenna is determined by Equation (2.1), where $R_p$ is a parallel resistance, $V_0$ is a voltage at the coil antenna, and $\eta$ is a characteristic impedance.

$$P_{rad} = \frac{\eta V_0^2}{2R_p} \tag{2.1}$$

The parallel resistance ($R_p$) is calculated by Equation (2.2), where Q is an antenna's quality factor, and $R_a$ is an available resistance.

$$R_p = \mathrm{Q}^2 R_a \tag{2.2}$$

The available resistance ($R_a$) is calculated by Equation (2.3), where $\omega_o$ is an angular frequency ($2\pi f$) and $L$ is the inductance of the coil antenna [10].

$$Q = \frac{\omega_o L}{R_a} = \frac{f_o}{BW} \tag{2.3}$$

Equation (2.4) is derived to calculate an inductance of a coil antenna from Equations (2.1), (2.2), and (2.3). Equation (2.4) presents the relationship between an inductance and an expected radiated power.

$$L = \frac{\eta V_0^2}{2Q\omega_o P_{rad}} \tag{2.4}$$

The antenna inductance is also determined by the dimension of a rectangular coil antenna. A length ($l$), a width ($w$) of an antenna, a trace width ($t$), a number of loops ($N$), and an electrical permittivity ($\mu$) influence the inductance of an antenna, shown in Equations (2.5) and (2.6) [11].

$$L = N\frac{\mu L}{\pi}\left[-2(w+l) + 2\sqrt{w^2+l^2} + C\right] \tag{2.5}$$

$$C = -l\ln\left(\frac{l+\sqrt{w^2+l^2}}{w}\right) - w\,ln\left(\frac{w+\sqrt{w^2+l^2}}{l}\right) + l\,ln\left(\frac{2l}{\frac{t}{2}}\right) + w\,ln\left(\frac{2w}{\frac{d}{2}}\right) \tag{2.6}$$

### 2.1.2. Impedance Matching

The impedance of an antenna should be matched to a low-impedance to transmit the expected power [5], [12]. Since bio-signals measured by the electronics have low amplitude signals, the impedance matching to 50 Ω provides the maximum power transfer between the radio frequency (RF) source and the loads. If the impedance is not matched, the reflected power is generated [11], [13], shown in

Equation (2.7).

$$P_{ref} = |\Gamma|^2 P_{inc} \tag{2.7}$$

The reflected power occurs as standing waves on the transmission line between the transmitter and the receiver. The forward and reflected waves can be added or subtracted depending on the phase between them. Therefore, the voltage is summed to zero and the maximum current occurs. The maximum current can damage or destroy the device [12]. The reflection coefficient (Γ) is calculated by Equation (2.8), where $Z_0$ is normally 50 Ω [13], [14].

$$\Gamma = \frac{Z - Z_0}{Z + Z_0} \tag{2.8}$$

The reflected power is negligible when the matched impedance ($Z$) is 50 Ω.

### 2.1.3. Series-to-Parallel/ Parallel-to-Series Transformation

The series-to-parallel transformation and the parallel-to-series transformation are used to find complex matching components. The series-to-parallel transformation is implemented to determine the parallel matching impedance components whereas the parallel-to-series transformation is implemented to determine the series matching impedance components [15].

In the series-to-parallel transformation, the bandwidth and the circuit quality (Q) factor is necessary to be considered at a certain frequency range. The Q factor is

calculated by series resistance ($R_s$) and reactance ($X_s$) for a circuit element at a particular frequency (Figure 2.1 (a)).

$$\mathrm{Q} = \frac{|X_s|}{R_s} \tag{2.9}$$

The equivalent parallel resistance ($R_p$) and reactance ($X_p$) are calculated by Equations (2.10) and (2.11).

$$R_p = R_s(1 + \mathrm{Q}^2) \tag{2.10}$$

$$X_p = X_s\left(1 + \frac{1}{\mathrm{Q}^2}\right) \tag{2.11}$$

The Q factor of the equivalent parallel circuit is the same as the Q factor of the original series representation [15].

The parallel-to-series transformation starts from the parallel impedance representation (Figure 2.1 (b)). The Q factor of the parallel impedance is given by Equation (2.12).

$$\mathrm{Q} = \frac{R_p}{|X_p|} \tag{2.12}$$

The equivalent series resistance and reactance are calculated by Equations (2.13) and (2.14).

$$X_s = \frac{X_p}{1 + \frac{1}{\mathrm{Q}^2}} \tag{2.13}$$

$$R_s = \frac{R_p}{1 + \mathrm{Q}^2} \tag{2.14}$$

The Q factor of the equivalent series circuit is the same as the Q factor of the original parallel representation [15].

## 2.2. Transmitter Antenna Circuit Design

### 2.2.1. Antenna Design

The dimension of the coil antenna for the transmitter needs to be selected based on the input radiated power. The antenna for the transmitter is supplied the power by a reader module (Feig Electronic), which provides the power of 12 W with the DC voltage of 8 V [16]. The Q factor at a frequency ($f_0$) of 13.56 MHz is determined by Equation (2.15), where a minimum operating bandwidth ($BW$) is 2 MHz [10], [15], [17].

$$\mathrm{Q} = \frac{f_0}{BW} = \frac{13.56\ MHz}{2\ \mathrm{MHz}} = 6.78 \tag{2.15}$$

The maximum antenna inductance is calculated by Equation (2.16).

$$L = \frac{120\pi(8\mathrm{V})^2}{2\times 6.78\times 2\pi(13.56\mathrm{MHz})\times 12\mathrm{W}} = 1.740\ \mathrm{uH} \tag{2.16}$$

The dimension of the transmitting antenna is selected by 30 cm x 30 cm (W x L) with a single loop and a trace width of 0.41 mm, shown in Figure 2.2. The theoretical antenna inductance of 1.56 uH is determined by HFSS (ANSYS)

simulation (Figure 2.3) [18]. Therefore, the antenna inductance of the transmitter based on the selected size does not exceed the maximum inductance of 1.740 uH.

A conductive material for the antenna should be selected based on its conductivity and its cost. Although silver and gold have higher conductivities than the copper, their costs is a lot more expensive than copper so that copper is commonly used for the antenna material [9]. Since copper is an efficient conductor of electrical energy with low cost, the copper wire with a diameter of 0.41 mm is used for the material of the antenna for the transmitter.

### 2.2.2. Impedance Matching

The three-element match is applied to determine the antenna impedance matching circuit. The network analyzer calibration is demonstrated by four RF test connectors: a short, an open, a 50-Ω load, and a low capacitance. The calibration removes parasitic effects of the fabricated antenna [17].

The antenna inductance is measured to 1.4991 uH with the antenna impedance of 2.149 + j153.25 Ω at the frequency of 13.56 MHz (Figure 2.4). The parallel resistance of the matching circuit at the minimum bandwidth of 2 MHz is calculated by Equation (2.17) [15], [17].

$$R_p = QX_L = Q(\omega L) = 6.78 \times 2\pi \times 13.56\text{MHz} \times 1.4991\text{uH} = 865.96\,\Omega \qquad (2.17)$$

The antenna for the transmitter and its matching circuit is shown in Figure 2.5. The measured impedance locates in the data point 1 (DP1), shown in Figure 2.6. A shunt (parallel) 23-pF capacitor shifts the impedance to the test point 2 (TP 2) and a shut (parallel) 1-kΩ resistor rotates the impedance from the test point 2 to the test point 3 (TP 3). Then, a 56-pF capacitor rotates the impedance from the test point 3 to the test point 4 (TP 4) and accomplishes the final impedance of 49.556 – j2.355 Ω, which can be considered as 50 Ω. The shut resistor, calculated to 865.96 Ω in Equation (2.17), is rounded up to 1 kΩ for yielding the match with capacitances. The impedance and the Q factor at each data point are shown in Table 3.2.

2.3. Figures

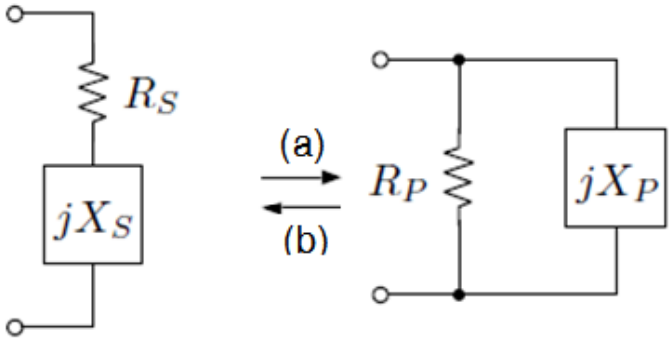


**Figure 2.1. The schematic of series and parallel impedance representations at a particular frequency: (a) the series-to-parallel transformation, and (b) the parallel-to-series transformation.**

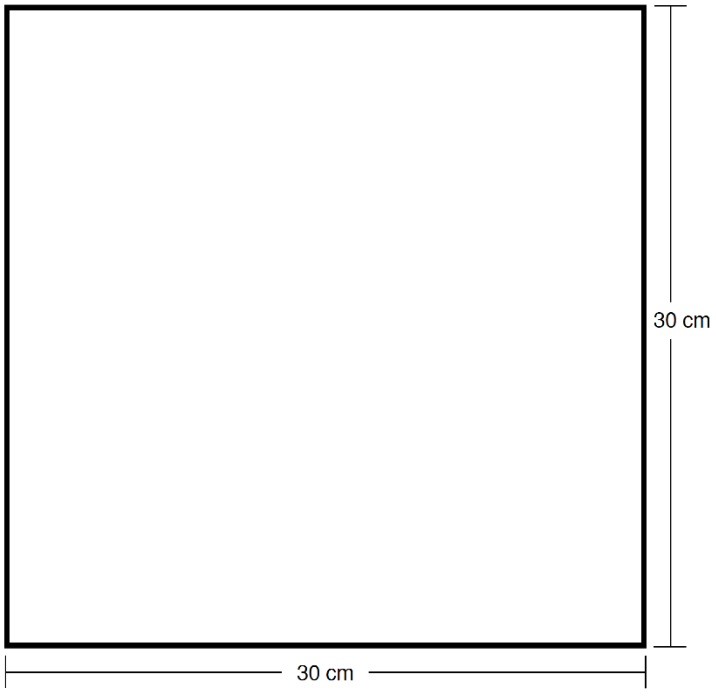


**Figure 2.2. The loop antenna design layout for the transmitter.**

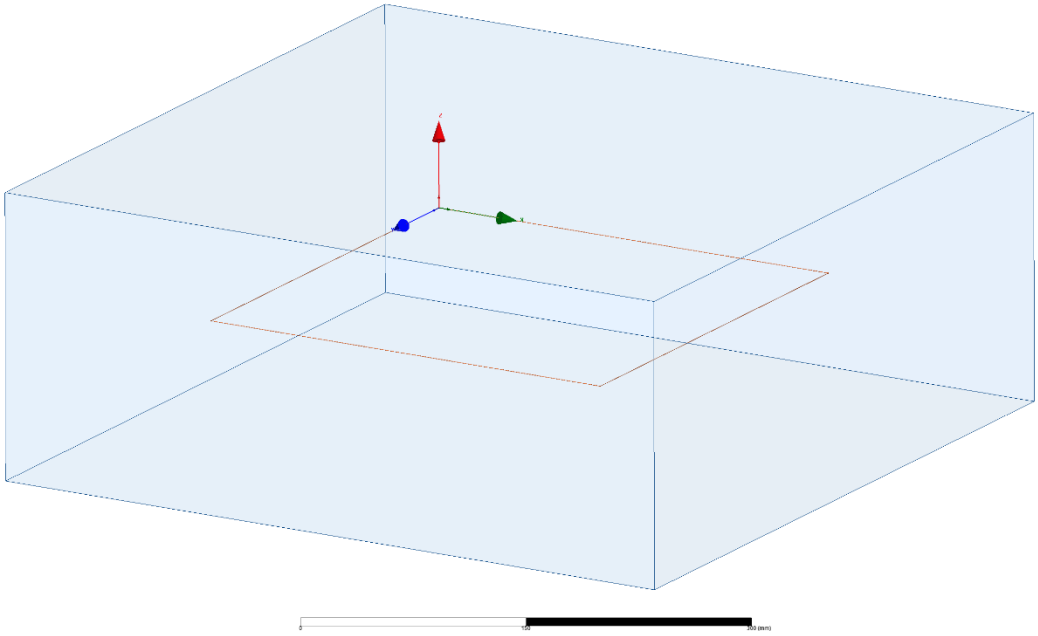

**Figure 2.3. HFSS antenna design for the transmitter. The trace of the antenna is composed of copper ($\epsilon_r = 1\ F/m,\ \mu_r = 0.999991\ H/m, \sigma = 5.8E7\ S/m, \rho = 8933\ kg/m^3$) and surrounded by airbox ($\epsilon_r = 1.0006\ F/m,\ \mu_r = 1.0000004\ H/m, \sigma = 0\ S/m, \rho = 1.1614\ kg/m^3$).**

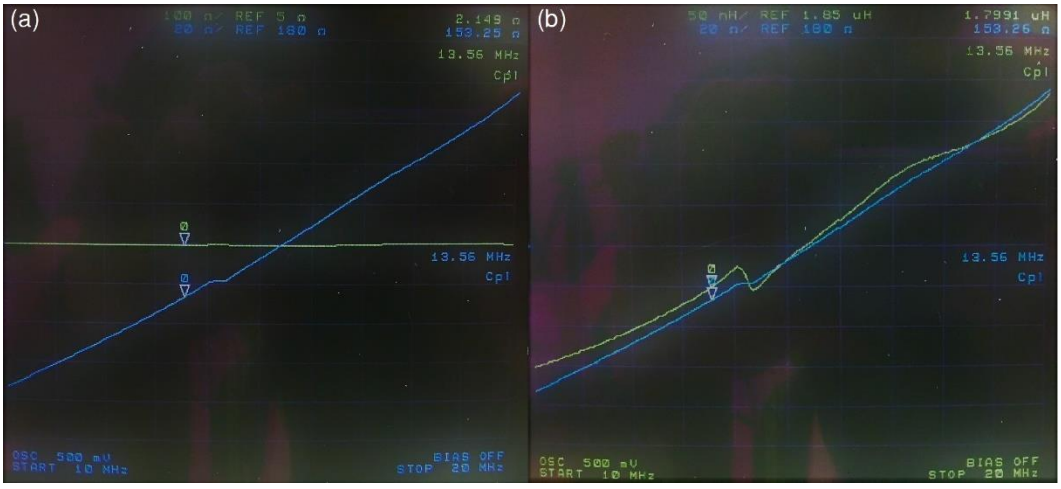


**Figure 2.4. (a) The measured impedance of the antenna for the transmitter and (b) the measured inductance of the antenna for the transmitter.**

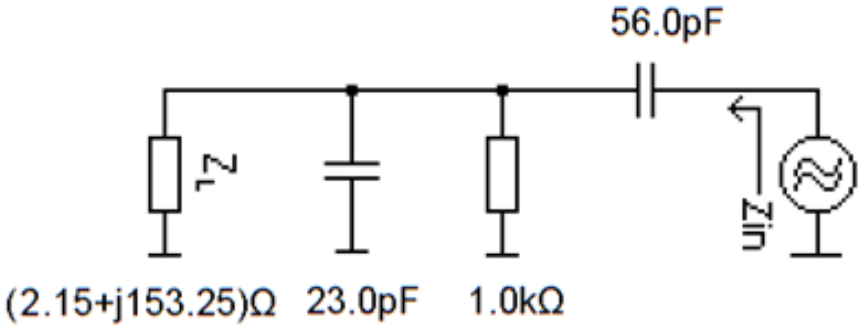


**Figure 2.5. Schematic of the impedance matching simulation of the antenna for the transmitter.**

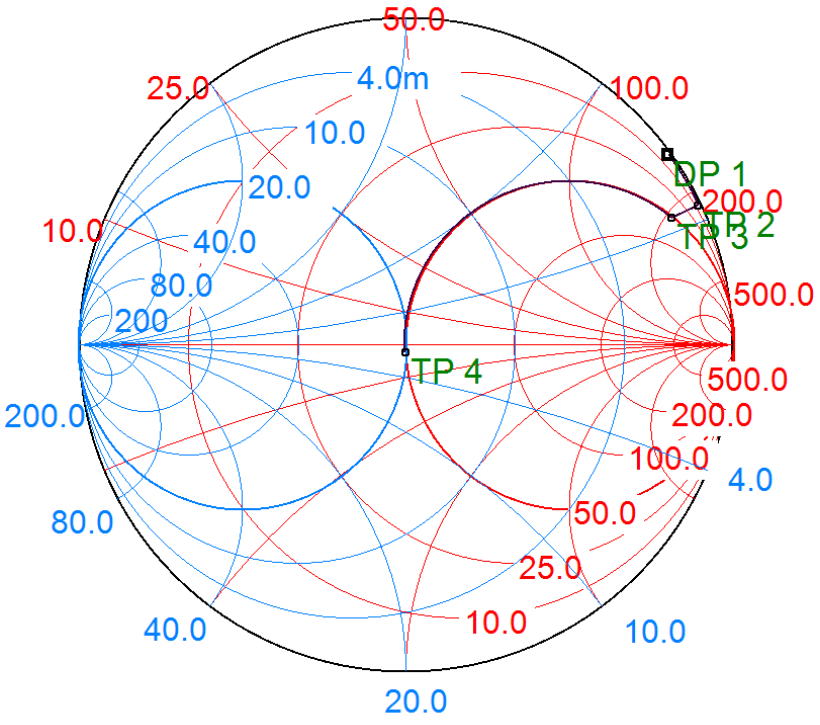


**Figure 2.6. Smith chart impedance matching of the antenna for the transmitter.**

2.4. Tables

**Table 2.1. Impedance and the Q factors of each data point in the Smith chart of the antenna matching simulation.**

| Point | Impedance (Ω) | Q factor | Frequency (MHz) |
|---|---|---|---|
| DP 1 | 2.149 + j153.25 | 71.312 | 13.56 |
| TP 2 | 4.389 + j218.999 | 49.892 | 13.56 |
| TP 3 | 49.556 + j207.236 | 4.182 | 13.56 |
| TP 4 | 49.556 - j2.355 | 0.048 | 13.56 |

# CAHPTER 3: RECEIVER ANTENNA CIRCUIT DESIGN

Chapter 3 introduces theoretical requirements of an antenna design for a receiver. The antenna for a receiver accepts the power from a coil antenna for a transmitter wirelessly and radiates the power to a bioelectronic system connected to a load. The receiving antenna matching method is different from the transmitting antenna matching method.

## 3.1. Theoretical Requirements

### 3.1.1. Quality Factors

Designing an antenna for a receiver has different aspects of consideration as a transmitting antenna. One of the important considerations is a quality (Q) factor. In general, the power received by an antenna is higher when a Q factor is higher. However, too high a Q factor conflicts with the band-pass characteristics of a reader and increases ringing, shown in Figure 3.1. Therefore, the Q factor should not exceed 20 [19]. The Q factor of the receiving antenna is calculated by Equation (3.1), where $R_p$ is a parallel resistance, $L$ is an antenna inductance, and $f_0$ is an operating frequency.

$$\mathrm{Q} = \frac{R_p}{2\pi f_0 L} \tag{3.1}$$

### 3.1.2. Resonance

Matching the impedance to 50 Ω is essential for a transmitting antenna circuit to transfer the power to a receiver without power loss. However, 50-Ω low impedance matching is not necessary for an antenna matching circuit for a receiver. Instead, the consideration of an antenna matching circuit for a receiver is to set the operation frequency to the resonant frequency. The maximum impedance is achieved at the resonance so that the power transferred from the transmitter is maximized [5]. The resonant frequency is achieved by a shunt (parallel) capacitor (*C*), shown in Equation (3.2).

$$f_o = \frac{1}{2\pi\sqrt{LC}} \tag{3.2}$$

Therefore, the capacitance of a shunt capacitor to operate the antenna circuit at resonance is calculated by Equation (3.3).

$$C = \frac{1}{(2\pi f_o)^2 L} \tag{3.2}$$

## 3.2. Receiver Antenna Circuit Design

### 3.2.1. Antenna Design

The dimension of the antenna design for the receiver is determined by the same method used to design the antenna for the transmitter [10]. The minimum power

accomplished by the receiving antenna should be at least 160~200 mW because eight bioelectronics, which consume the power of 15 ~ 20 mW each, are attached to the receiver. The voltage across each bioelectronic is 2.5~3 V, the optimized voltage of a bioelectronic operation. The Q factor at a frequency of 13.56 MHz is estimated to be the maximum Q factor of 20 for the antenna inductance calculation. The maximum antenna inductance of the receiver is calculated by Equation (3.4).

$$L = \frac{120\pi(3\text{V})^2}{2\times20\times2\pi(13.56\text{MHz})\times0.16\text{W}} = 6.22 \text{ uH} \quad (3.4)$$

The dimension of the antenna for the receiver, shown in Figure 3.2, is selected by 7.5 cm x 7.5 cm (W x L) with four loops, the trace width of 0.6 cm, and the spacing of 0.1 cm. The theoretical antenna inductance for the receiver is 3.88 uH, determined by HFSS simulation (Figure 3.3) [18]. Therefore, the antenna inductance of the receiver based on the selected dimension of the coil does not exceed the maximum inductance of 6.22 uH.

### 3.2.2. Fabrication Process

Since copper is also selected for the material of the receiving coil antenna based on its conductivity compared to its cost [9], the coil antenna for the receiver is fabricated on an 18 um-copper polyimide film (Pyralux Copper Clad Laminates, Dupont) with a sacrificial substrate of a glass microslide (Figure 3.4 (a)), followed

photolithography. The positive photoresist (AZ 4620, MicroChemicals) is spin-coated (Figure 3.4 (b)) and soft-baked at 110 °C. The coated substrate placed under the coil antenna layout pattern undergoes the ultraviolet (UV) exposure. The photoresist is developed by the developer (AZ 400 K, MicroChemicals), diluted with water (Figure 3.4 (c)), and then the copper is wet-etched (Figure 3.4 (d)). The specific conditions of the fabrication process are shown in Table 3.1.

### 3.2.3. Resonance Matching

The resonant frequency of the coil antenna for the receiver is determined to a frequency of 13.56 MHz because the wireless power transfer is achieved at the near-field communication operating frequency. Since the theoretical Q factor calculated by theoretical antenna impedance of 9.45 + j330.76 Ω exceeds the maximum Q factor, the 20-Ω resistor is added in the series connection. The expected theoretical impedance becomes 29.45 + j330.76 with the Q factor of 11.23 at the frequency 13.56 MHz.

The measured antenna inductance for the receiver is 5.0347 uH and the measured antenna impedance for the receiver is 37.04 + j425.56, shown in Figure 3.5. Therefore, the capacitance, calculated by Equation (3.5), is parallelly connected to operate the circuit at the frequency of 13.56 MHz, shown in Figure 3.6 [19].

$$\mathrm{C} = \frac{1}{(2\pi f_o)^2 L} = \frac{1}{(2\pi \times 13.56\mathrm{MHz})^2 \times 5.0347\mathrm{uH}} = 27.36\ \mathrm{pF} \qquad (3.5)$$

The Q factor based on the measured antenna impedance is 11.48, which does not exceed 20.

The data point of the measured impedance of the coil antenna for the receiver on the Smith chart is shown in Figure 3.7 as DP1. The impedance is rotated to the test point 2 (TP 2) by a shunt 27-pF capacitor rotates and becomes 4808.542 + j752.762 Ω. The final impedance of the receiving coil antenna matching circuit is considered as open, the maximum impedance. The impedance and the Q factor at each data point are shown in Table 3.2.

3.3. Figures

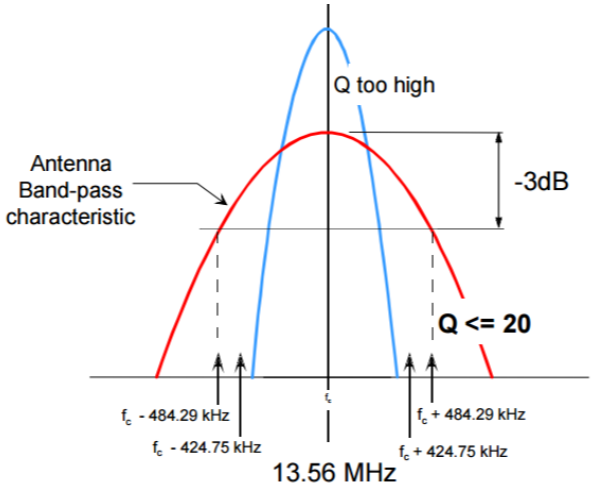


**Figure 3.1. Antenna Q factor curves. When Q is too high (> 20), the ringing is increased and results in the problems in the protocol bit timing [19].**

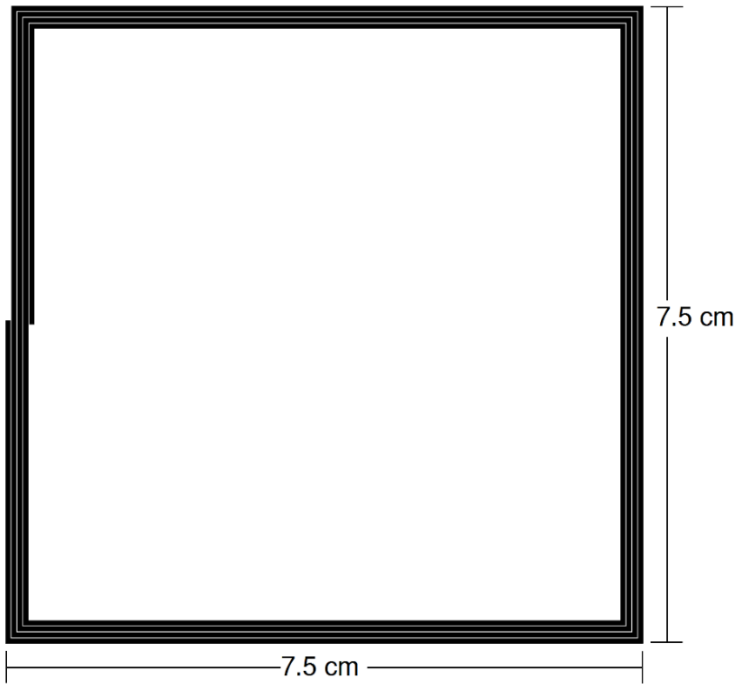


**Figure 3.2. Coil antenna design layout for the receiver.**

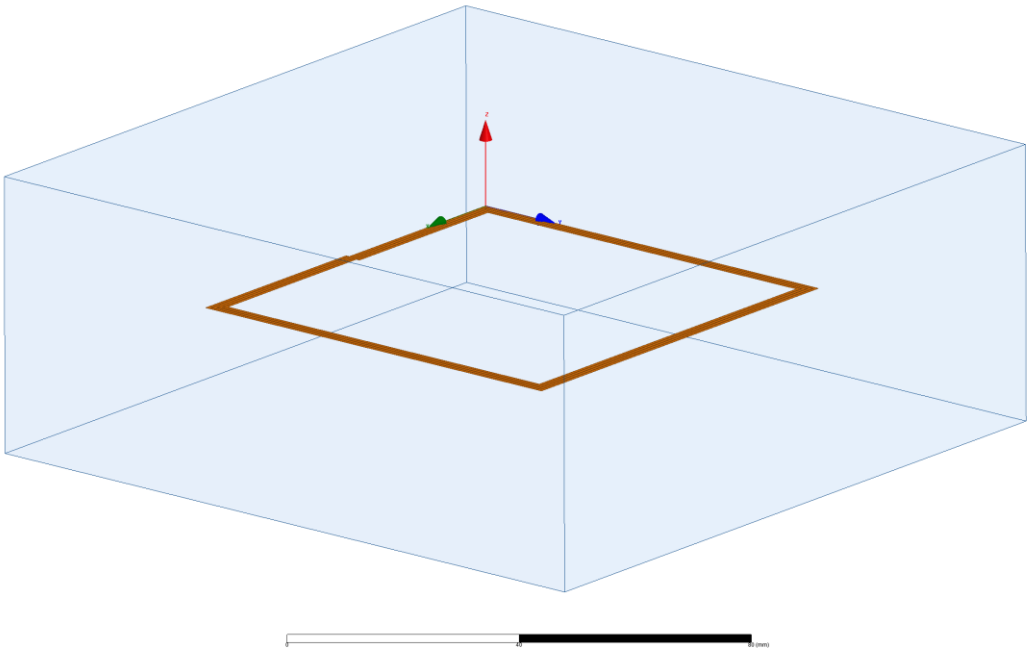

**Figure 3.3. HFSS coil antenna design for the receiver. The trace of the antenna is composed of copper ($\epsilon_r = 1\ F/m,\ \mu_r = 0.999991\ H/m, \sigma = 5.8E7\ S/m, \rho = 8933\ kg/m^3$) and surrounded by airbox ($\epsilon_r = 1.0006\ F/m,\ \mu_r = 1.0000004\ H/m, \sigma = 0\ S/m, \rho = 1.1614\ kg/m^3$).**

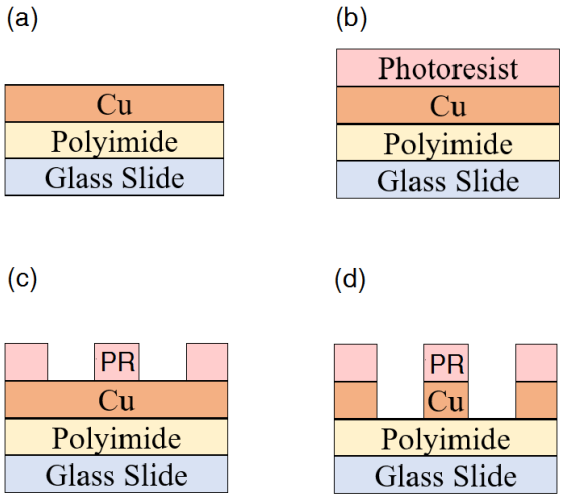


**Figure 3.4. Fabrication procedure steps of the coil antenna for the receiver.**

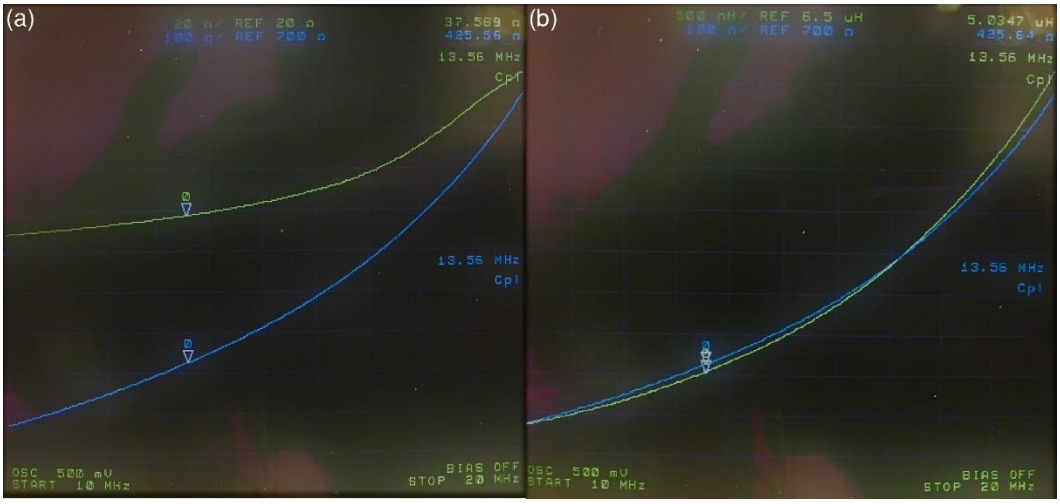


**Figure 3.5. (a) The measured impedance of the coil antenna for the receiver and (b) the measured inductance of the coil antenna for the receiver.**

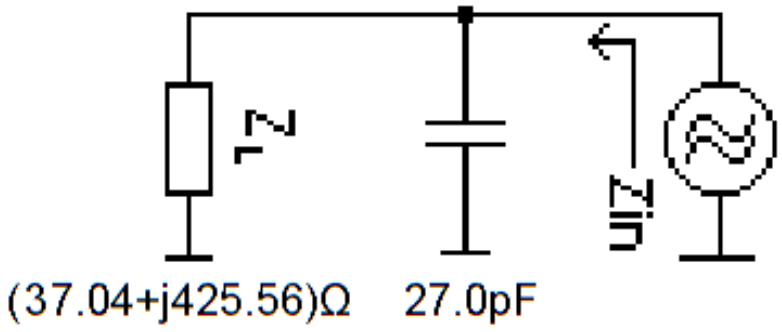


**Figure 3.6. Schematic of the coil antenna matching circuit simulation for the receiver.**

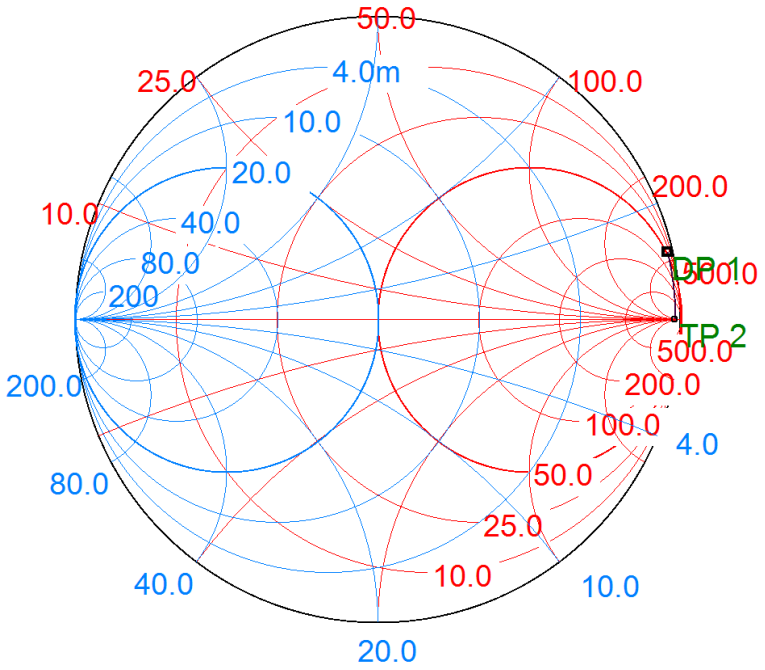


**Figure 3.7. Smith chart impedance matching of the antenna for the receiver.**

3.4. Tables

**Table 3.1. Fabrication conditions of the antenna.**

| | |
|---|---|
| Spin-coating rate/ ramp (RPM) | 3000/ 1000 |
| Spin-coating time (sec) | 30 |
| Soft-bake at 110 °C (sec) | 90 |
| Exposure (sec) | 30 |
| Development (sec) | 60 ~ 75 |
| Copper etching (sec) | 180 ~ 270 |

**Table 3.2. Impedance and Q factors of each data point in the Smith chart of the antenna matching simulation.**

| Point | Impedance (Ω) | Q | Frequency (MHz) |
|---|---|---|---|
| DP 1 | 37.040 + j425.560 | 11.489 | 13.56 |
| TP 2 | 4808.542 + j752.762 | 0.157 | 13.56 |

# CHAPTER 4: BIOELECTRONIC APPLICATION: ACTUATOR

Chapter 4 introduces a bioelectronic application of the wireless power transfer achieved by the transmitter and the receiver antenna matching circuit. The actuation sensor in the system receives the power from the coil antenna matching circuit for the receiver and controlled by an NFC transponder and a bilateral switch.

## 4.1. Actuation System Design

The actuation system consists of two coil antennas, actuators, an NFC transponder (RF430FRL, Texas Instruments), bilateral switches (74LVC1G384, Nexperia), diodes, capacitors, and actuation sensors, shown in Figure 4.1. The received power from the large (L) coil antenna is delivered to an actuation sensor. The antenna L design is matched with a shunt 27-pF capacitor to set the resonant frequency at 13.56 MHz. The small (S) coil antenna provides the power to operate the NFC transponder at the NFC operating frequency. The power required to activate the NFC transponder is 200 mW with a supply voltage of 3.6 V [20]. The maximum antenna inductance of the antenna S is determined by Equation (4.1) [10].

$$L = \frac{120\pi(3.6\text{V})^2}{2\times20\times2\pi(13.56\text{MHz})\times0.2\text{W}} = 7.168\ \text{uH} \tag{4.1}$$

The antenna S with a diameter of 3.5 cm, five loops, the trace width of 0.6 cm, and the spacing of 0.1 cm has the theoretical antenna inductance of 3.72 uH, calculated

by Equations (2.5) and (2.7). Therefore, the antenna inductance of the antenna S is acceptable since it does not exceed the maximum inductance of 7.168 uH. Since the impedance of the antenna S is 6.12 + j318 Ω, a 15-Ω resistor is connected to lessen the Q factor to 15.06. The antenna S is fabricated on an 18 um-copper polyimide film.

The measured inductance of the small coil antenna is 3.83 uH. The NFC link is applied to receive the power from the transmitter wirelessly. Therefore, a shunt capacitor, calculated by Equation (4.2), is required to operate the small coil antenna at a frequency of 13.56 MHz.

$$\mathrm{C} = \frac{1}{(2\pi f_o)^2 \times L} = \frac{1}{(2\pi \times 13.56\mathrm{MHz})^2 \times 3.83\mathrm{uH}} = 36\ \mathrm{pF} \qquad (4.2)$$

Since the NFC transponder chip has an adjustable input capacitance of 31.5 ~ 38.5 pF [20], an additional 36-pF capacitor is not necessary to be attached parallelly to the small coil antenna.

There are seven actuation sensors placed on the single actuation system. Each actuation sensor is controlled by a bilateral switch, which converts its state determined by the NFC transponder chip. A general-purpose digital input and output terminal (GPIO) signal from the NFC transponder determines an enable bit of the bilateral switch. The GPIO signal ($V_{IO}$) provides a 200 Hz square wave to the bilateral switch (Figure 4.2), where $V_{high} \approx 1.5\ \mathrm{V}$ and $V_{low} \approx 0\ \mathrm{V}$ [19]. Since

the bilateral switch is an active low logic [21], the switch is on-state at low GPIO voltage and off-state at high GPIO voltage. The NFC transponder has the total of eight GPIO ports to control eight actuation sensors independently [20]. The data exchange format (NDEF) is encoded into the NFC transponder to decide a shape, an amplitude and a frequency of the GPIO signal. NDEF also allows the NFC transponder to communicate the data with a PC.

The bilateral switch regulates the signal to be provided or blocked to the actuation sensor. When the switch is on-state, the current from the antenna L flows through the switch and reaches to the actuation sensor. In the other way, the current cannot be passed through the sensor when the switch is off-state.

### 4.2. Actuation Sensor Design

An actuation sensor is composed of a copper coil, a cylindrical magnet, a layer of Polydimethylsiloxane (PDMS), and a thin polyimide (PI) film, shown in Figure 4.3 and Figure 4.4. The 18-um copper coil locates at the bottom of the sensor and the cylindrical magnet is placed on the coil. The resonance is presented in the copper coil at a frequency of 13.56 MHz by the parallel-connected adjustable capacitor from the NFC transponder chip. A small air gap exists between the magnet and the coil to allow a space for the vibration of the magnet. A flexible 12-um PI film, supported by the 3-mm PDMS layer, is attached to the magnet to endure the

vibration of the magnet and. PDMS is a soft, flexible and stretchable material which prevents the actuation sensor from any damage that might occur by vibration of the magnet. Moreover, PDMS implements the air gap between the coil and the magnet.

The actuation sensor is a moving magnet actuator (MMA) operated by the electromagnetic field. When the conductive coil acquires the current ($I$) from the long coil antenna, the electromagnetic field, produced by the electric field $\overrightarrow{(E)}$ and the magnetic field ($\vec{B}$), is generated [22].

$$\vec{E} = \frac{\eta_o I}{2\pi r}\hat{\theta} \tag{4.3}$$

$$\vec{B} = \frac{\mu_o I}{2\pi r}\hat{\phi} \tag{4.4}$$

The electromagnetic field produces the Lorentz force ($\vec{B}$), calculated by Equation (4.5) [22], [23].

$$\vec{B} = \mathrm{q}\vec{E} + q\vec{v}\times\vec{B} \tag{4.5}$$

The Lorentz force leads the magnet, sandwiched by the copper coil and the PI film, to move up over a range of a few micrometers. The motion of the magnet is a frictionless and a backlash-free motion [23]. When the switch is off-state, the current is blocked to the copper coil and the electromagnetic field is degenerated and the Lorentz force no longer exists. Then, the magnet moves down and resumes to its original state.

There are many applications of the moving magnet actuation sensor: precision motion systems, disk drives, and automotive valves [23]. The actuation sensor is also applied to skin-mountable bioelectronic systems. One of bioelectronic applications is the virtual reality (VR) systems, a three-dimensional computer-generated environment system which allows people to manipulate objects and to perform series of actions in the virtual reality world. The virtual reality has many applications such as architecture, sport, medicine, and entertainment [24]. The actuation system is primarily used for the entertainment purpose in the virtual reality system. Because the actuation system is mountable to the skin, the system can be applied to design accessories for entertaining in the virtual reality world.

4.3. Figures

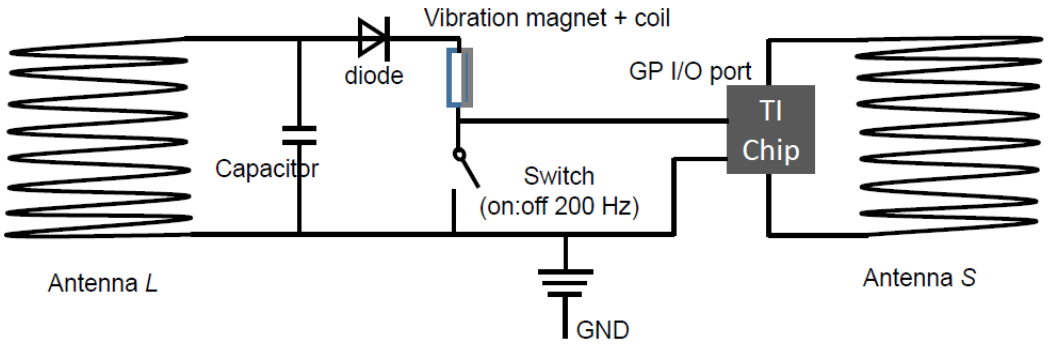


**Figure 4.1. The actuation system design for a single actuation sensor. The actuation system consists of seven actuation sensors.**

| GPIO voltage | IC switch state | $V_{out}$ voltage |
|---|---|---|
| High | Off | Low |
| Low | On | High |

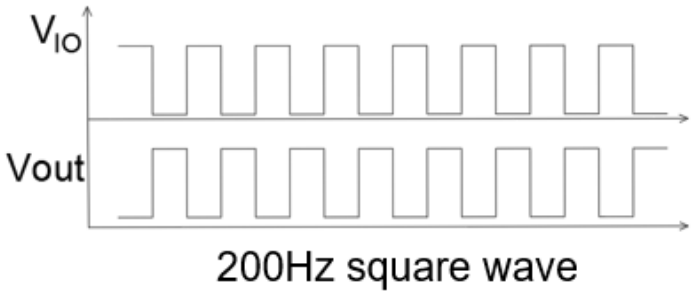


**Figure 4.2. The 200-Hz square wave of GPIO from the NFC transponder chip and the outgoing wave of the bilateral switch.**

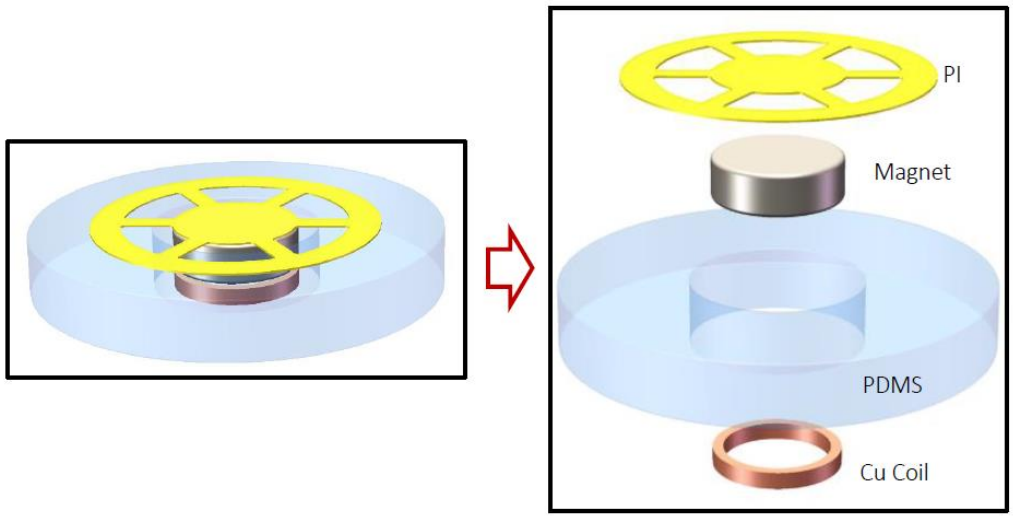


**Figure 4.3. Picture of the actuation sensor. The actuation sensor is composed of a copper coil, a magnet, and a thin PI film covered by PDMS.**

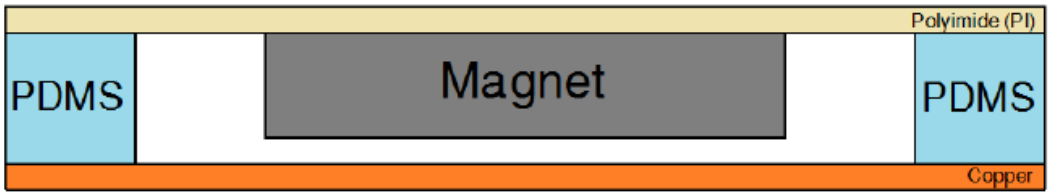


**Figure 4.4. Cross section of the single actuation sensor.**

# CHAPTER 5: RESULTS AND DISCUSSION

## 5.1. Results: Transmitter Antenna Design

### 5.1.1. Matching Simulation Results

The transmitting antenna matching circuit simulation is demonstrated in Advanced Design System (ADS, Keysight Technologies) with a frequency sweep of 100 kHz ~ 20 MHz, and a step frequency of 10 kHz (Figure 5.1) [25]. The single port excitation generates the complex S11 parameter of the antenna matching circuit. The input impedance is calculated with the S11 parameter by Equation (5.1) [26].

$$Z_{in} = Z_0\left(\frac{1+S_{11}}{1-S_{11}}\right) = Z_0\left(\frac{1+R+jX}{1-R-jX}\right) = Z_0\left(\frac{1-R^2-X^2+j2X}{(1-R)^2+X^2}\right) \quad (5.1)$$

The real ($R$) and the imaginary ($X$) components of the input impedance are determined in Equations (5.2) and (5.3) [27].

$$Z_{in,real} = Z_0\left(\frac{1-R^2-X^2}{(1-R)^2+X^2}\right) \quad (5.2)$$

$$Z_{in,imaginary} = Z_0\left(\frac{2X}{(1-R)^2+X^2}\right) \quad (5.3)$$

Since the real S11 parameter ($R$) of the matching circuit is 0.004 and the imaginary S11 parameter ($X$) of the matching circuit is 0.023 at a frequency of 13.56 MHz (Figure 5.2), the simulated matched impedance of the transmitting coil antenna based on the measured antenna impedance is 49.584 - j2.296 Ω at a frequency of

13.56 MHz (Figure 5.3). In addition, the matched antenna circuit impedance locates at the center of the Smith chart at a frequency of 13.56 MHz (Figure 5.4). Therefore, the matched impedance for the transmitter at a frequency of 13.56 MHz is comparable to 50 Ω.

The dB curve of the S11 parameter demonstrates 10 dB return loss of the transmitting antenna matching circuit over a 1.53 MHz bandwidth (Figure 5.5). The 3-dB bandwidth of the antenna is calculated by Equation (5.4) [17].

$$BW_{3dB} = 2BW_{10dB} = 3.06 \text{ MHz} \tag{5.4}$$

Therefore, the 3-dB bandwidth satisfies the condition of the minimum operating bandwidth of 2 MHz.

### 5.1.2. Measurement Results

The shunt 23-pF capacitor, and the shut 1-kΩ resistor, and the series 56-pF capacitor are connected to the antenna to match the transmitting antenna circuit impedance to 50 Ω. The measured impedance of the antenna for the transmitter, shown in Figure 2.4, is used for the antenna impedance of the transmitter. The matched impedance of the transmitting coil antenna circuit is 49.577 – j1.369 Ω, shown in Figure 5.6. The return loss (RL) of the transmitter coil antenna is calculated by Equation (5.8), where $Z_0$ is 50 Ω [14].

$$\text{RL (dB)} = -20\log\sqrt{\frac{(R_{in}-Z_0)^2+{X_{in}}^2}{(R_{in}+Z_0)^2+{X_{in}}^2}} = -84.83\ \text{dB} \quad (5.5)$$

Since the loss of the coil antenna does not exceed -13 dB [27], the return loss of antenna matching circuit for the transmitter does not affect the transmitted signals.

## 5.2. Results: Receiver Antenna Design

### 5.2.1. Simulation Results

The ADS simulation of the receiving antenna matching circuit, shown in Figure 5.7, with a frequency range of 100 kHz ~ 20 MHz and a frequency step of 10 kHz [25] determines the resonant frequency of the matching circuit. The shunt 27-pF capacitor is connected to operate the wireless power transfer at the frequency of 13.56 MHz. The real S11 parameter ($R$) of 0.981 and the imaginary S11 parameter ($X$) of 0.001 at a frequency of 13.56 MHz (Figure 5.8) is used to calculate the impedance of the receiving antenna matching circuit to 4982 + j338.727 Ω (Figure 5.9), derived from Equations (5.4) and (5.5) [26]. The receiving coil antenna matching circuit impedance locates at the right side of the Smith chart at a frequency of 13.56 MHz (Figure 5.10). Therefore, the matched impedance for the transmitter at 13.56 MHz is comparable to the infinite impedance. The maximum power is delivered to the receiving coil antenna circuit according to the high voltage across the load.

### 5.2.2. Measurement Results

The shunt 27-pF capacitor is connected to the coil antenna for the receiver to achieve the wireless power transfer at the frequency of 13.56 MHz. The measured impedance of the antenna for the receiver, shown in Figure 3.5, is used for the antenna impedance of the transmitter. The impedance of the receiving coil antenna circuit at resonance is 4770.5 + j557.57 Ω at the frequency of 13.56 MHz (Figure 5.11 (a)). Since the magnitude of the antenna impedance has a peak maximum at a frequency of 13.56 MHz (Figure 5.11 (b)), the resonance of the receiving coil antenna circuit presents at the frequency of 13.56 MHz.

The picture, shown in Figure 5.12, is a circuit for the power measurement radiated by the receiving coil antenna at the load. The AC voltage provided by the receiving coil antenna is rectified to the DC voltage to allow being measured by a multimeter. A Schottky diode (BAS40L, Nexperia) and a shunt (parallel) 1-uF capacitor is connected to the receiving antenna matching circuit to form a half-wave rectifier. Then, a 1-kΩ resistor is parallelly connected to the half-wave rectifier to determine the power at the load, determined by Equation (5.6) [13]. Figure 5.13 shows the change of the radiated power at the load by the change of communication distance between the transmitting antenna and the receiving antenna, where the input power at the transmitter is 12 W. The receiving coil antenna matching circuit is placed in the center of the transmitting coil antenna and lifted to measure the radiated power

varied by the communication distance. The radiated power decreases by the increase of the communication distances. Shown in Table 5.1, the power is enough to be reached the minimum power requirement of 160 ~ 200 mW for bioelectric system operation at the maximum communication distance of 10 ~ 15 cm.

The power efficiency of the inductive link system by coil antennas demonstrates the ratio between the input power from the transmitter and the output power at the receiver [13].

$$\eta = \frac{P_{out}}{P_{in}} \tag{5.6}$$

The power efficiency diminishes when the communication distance becomes longer, shown in Table 5.1. Therefore, the receiving antenna matching circuit is better placed close to the transmitter to receive the power with higher efficiency.

## 5.3. Actuation System Results

The actuation system is attached to the load of the receiving coil antenna matching circuit and delivered the power by the receiving coil antenna. The AC voltage from the receiving antenna is rectified by a diode and then provided to the actuation sensor. The voltage is also regulated to 2.5 ~3.0 V to be achieved in the acceptable range for the voltage of the actuation sensor. When the actuation sensor is activated, the movement of the cylindrical magnet (as high as 2 mm) is observed at the lower

frequency ($< 20$ Hz) whereas the vibration of the magnet is observed at the high frequency ($\approx 200$ Hz). The frequency and the square-shape of the wave at the terminal of the actuation sensor maintain the same as before and after connecting the coil. However, the output voltage of the square wave is dropped by the present of the coil connection at the terminal because of the power consumption by the actuation sensor and the self-induced electromotive force of the coil.

The picture of the actuation system is shown in Figure 5.14. The actuation system without any capsulation of additional soft, flexible, and stretchable materials can be torn or damaged if the system is attached to the skin. Therefore, a soft and flexible fabric is attached on the bottom and a 200-um layer of PDMS is spin-coated on the top to passivate the system. The capsulated actuation system prevents the damage from the outside force to stretch or bend the system, shown in Figure 5.15. The fabric and the layer of PDMS also allow the system to be reusable and waterproof on the human skin.

5.4. Figures

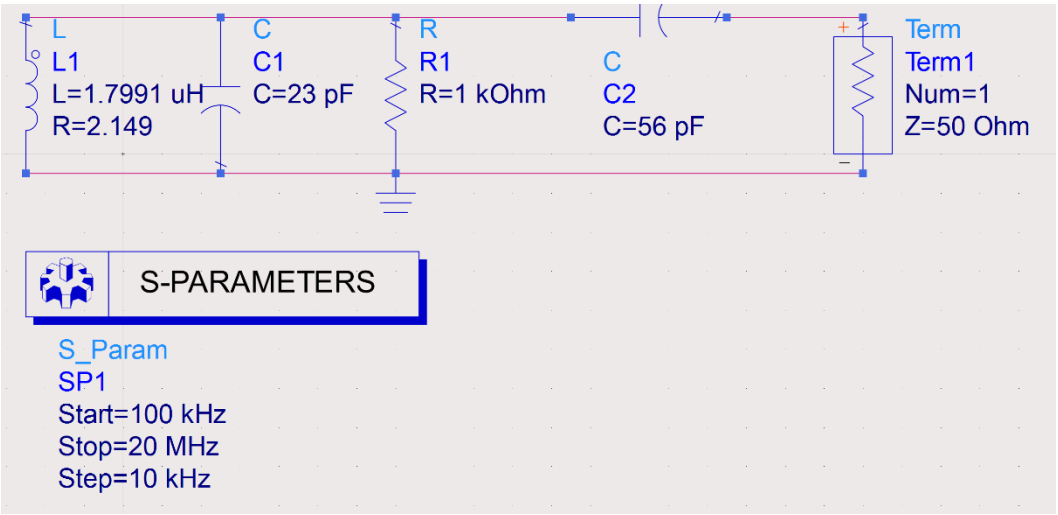


**Figure 5.1. Schematic of the antenna matching circuit for the transmitter in Advanced Design System 2016.01.**

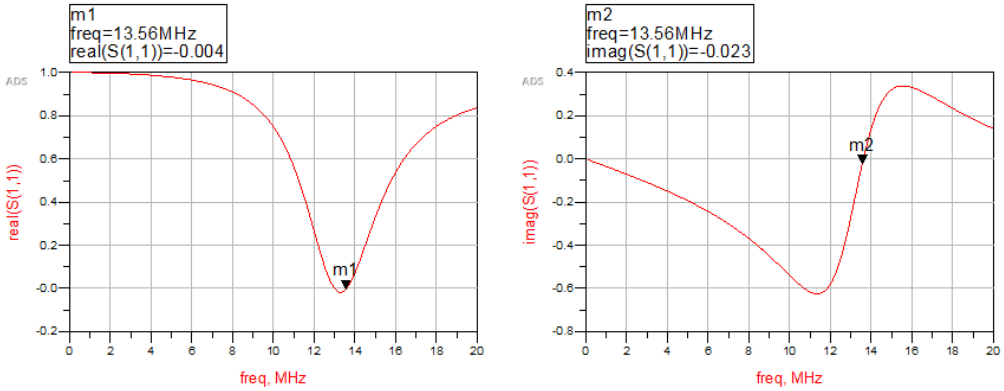


**Figure 5.2. Real and imaginary S11 parameter curves of the antenna matching circuit for the transmitter.**

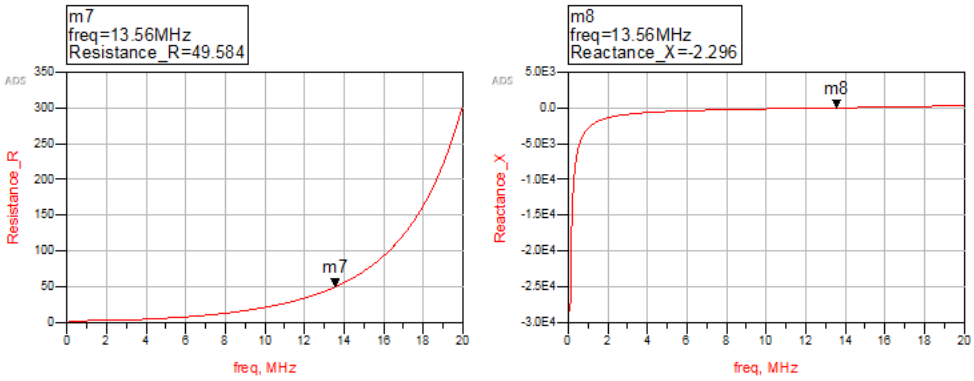


**Figure 5.3. Real and imaginary impedance curves of the antenna matching circuit for the transmitter.**

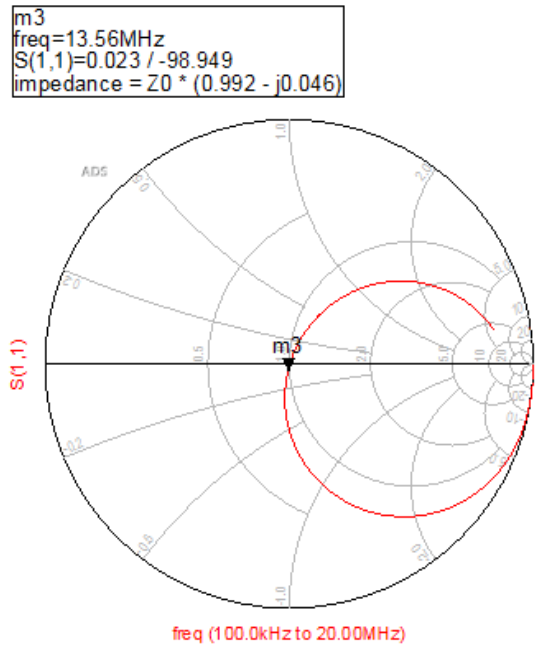


**Figure 5.4. Smith chart of the S11 parameter for the transmitting antenna matching circuit. M3 locates in the center of the Smith chart ($Z_{in} \approx 50\Omega$) at a frequency of 13.56 MHz.**

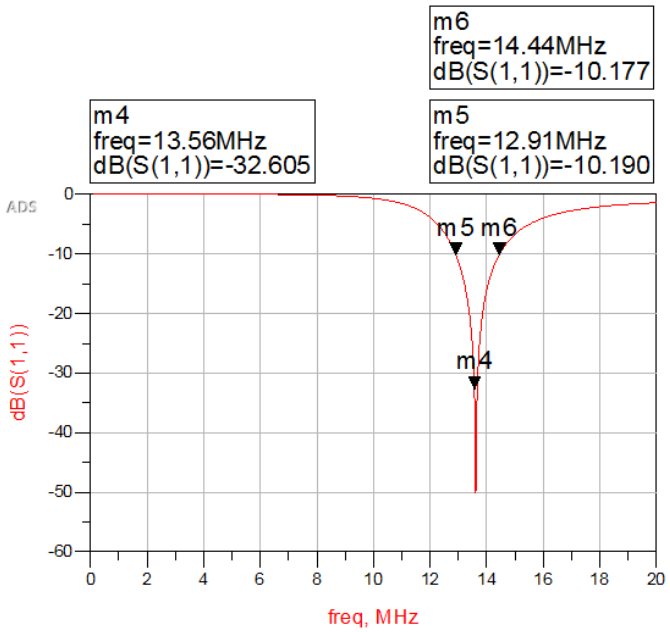


**Figure 5.5. The S11 parameter in dB of the antenna matching circuit for the transmitter. The 10-dB return loss bandwidth is the frequency difference between M5 and M6.**

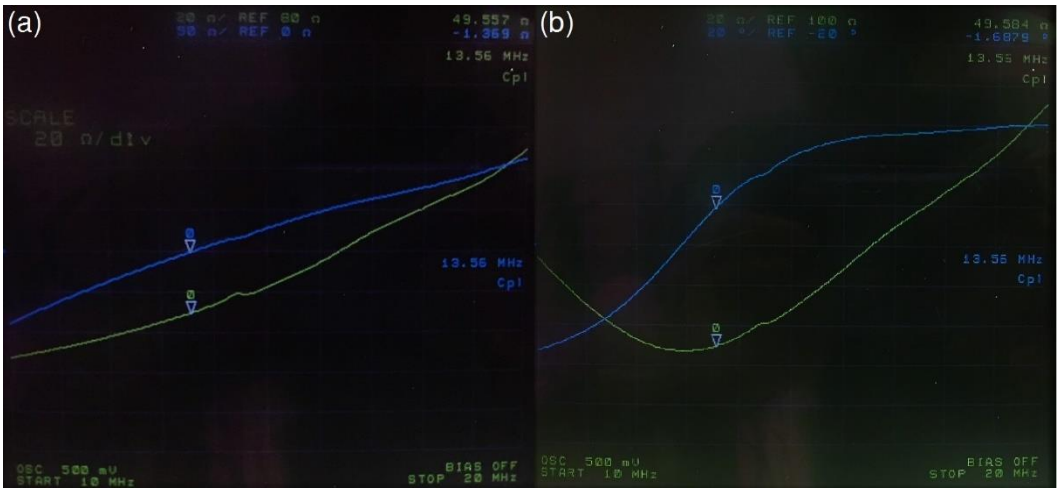


**Figure 5.6. (a) The impedance of the antenna matching circuit for the transmitter in a rectangular form and (b) the impedance of the antenna matching circuit for the transmitter in a polar form.**

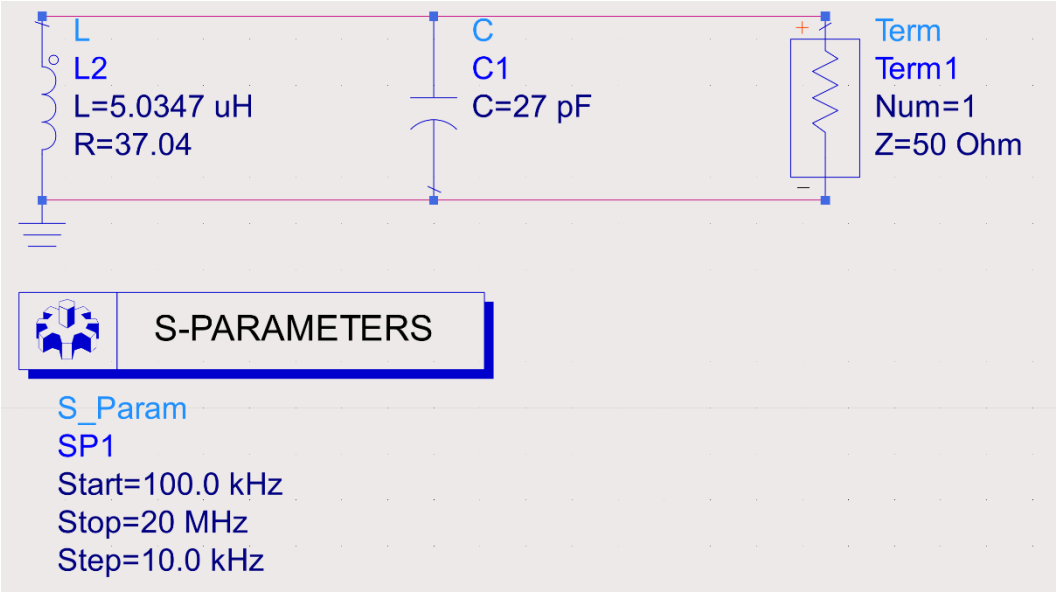


**Figure 5.7. Schematic of the antenna matching circuit for the receiver in Advanced Design System 2016.01.**

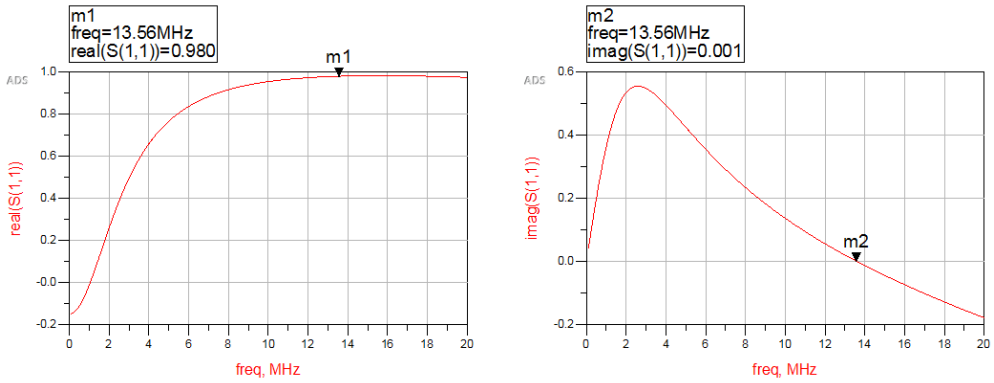


**Figure 5.8. Real and imaginary S11 parameter curves of the antenna matching circuit for the receiver.**

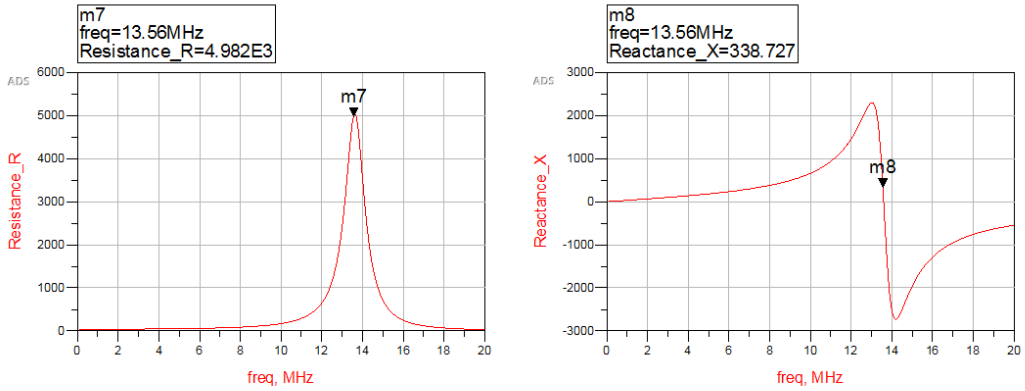


**Figure 5.9. Real and imaginary impedance curves of the antenna matching circuit for the receiver.**

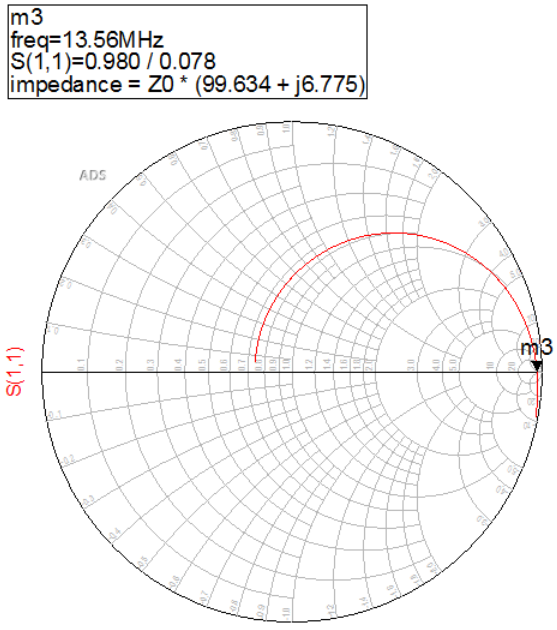


**Figure 5.10. Smith chart of the S11 parameter for receiving antenna matching circuit. M3 locates on the right side of the Smith chart ($Z_{in} \approx \infty$) at a frequency of 13.56 MHz.**

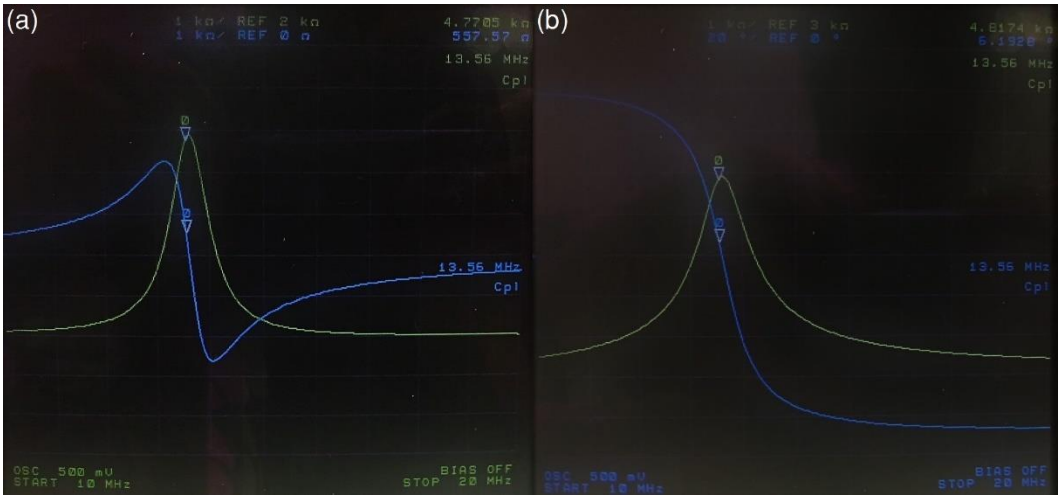


**Figure 5.11. (a) The impedance of the antenna matching circuit for the receiver in a rectangular form and (b) the impedance of the antenna matching circuit for the receiver in a polar form.**

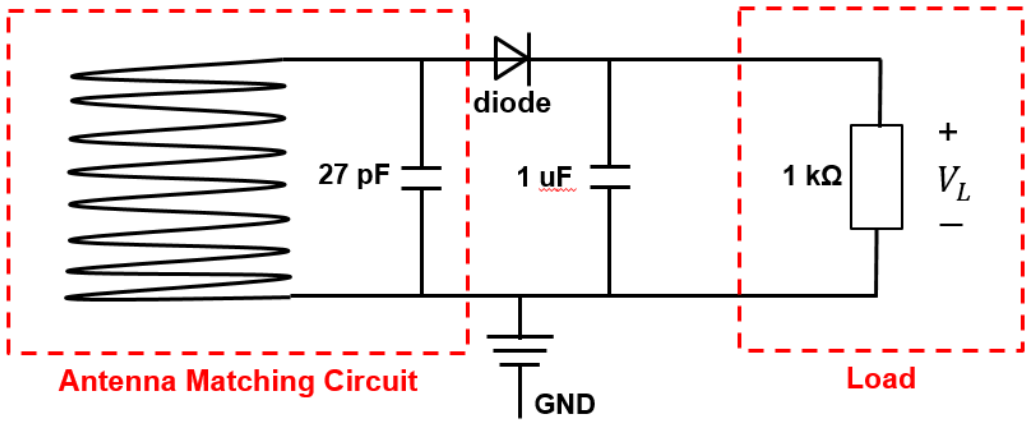


**Figure 5.12. The circuit diagram to determine the radiated power at the load in different communication distance between the transmitter and the receiver.**

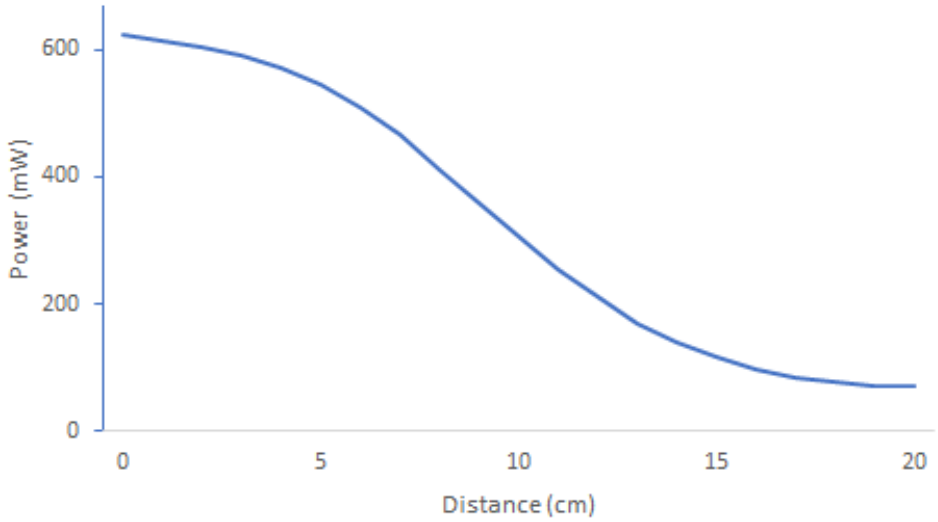


**Figure 5.13. The results of the change in the radiated power by the communication distance between the transmitter and the receiver.**

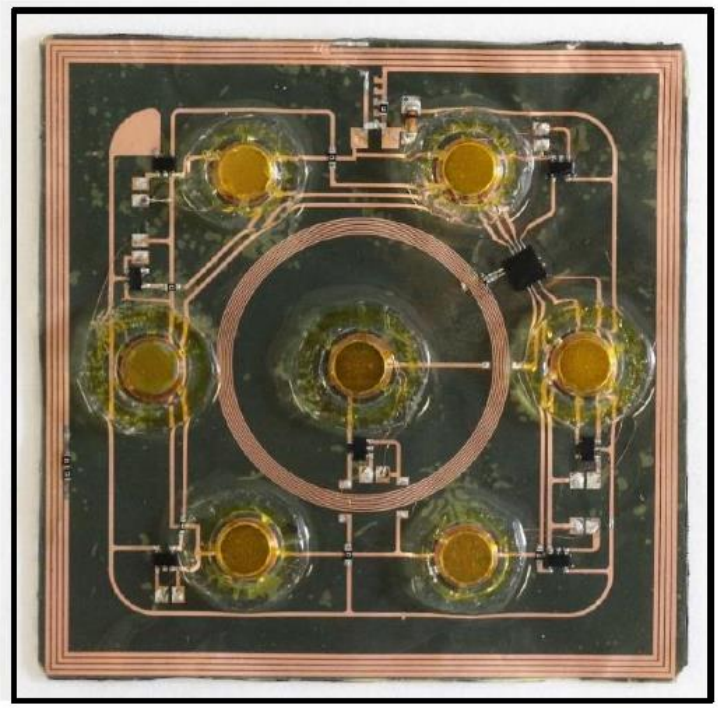

**Figure 5.14. Picture of the actuation system. The actuation system consists of seven actuation sensors and the receiving coil antenna matching circuit.**

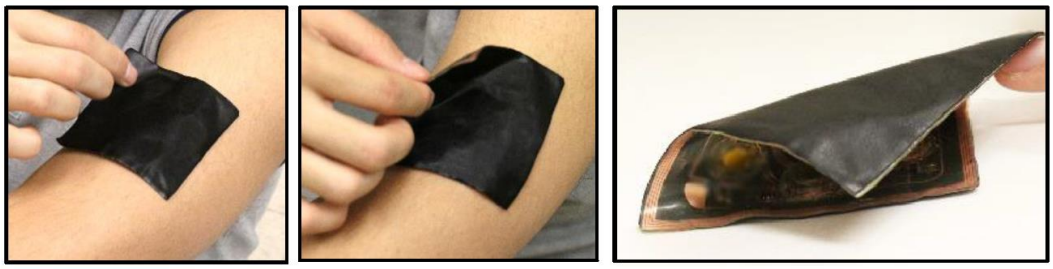

**Figure 5.15. The actuation system circuit in stretched and twisted views to demonstrate the stretchability and flexibility.**

5.5. Tables

**Table 5.1. Radiated power and the power efficiency by the increase of communication distance.**

| Communication Distance (cm) | Power (mW) | Efficiency |
|---|---|---|
| 0 | 623.00 | 0.052 |
| 5 | 544.76 | 0.045 |
| 10 | 306.95 | 0.026 |
| 15 | 119.25 | 0.010 |
| 20 | 70.067 | 0.006 |

# CHAPTER 6: CONCLUSION

In this thesis, a transmitting and receiving antenna design and their matching methods have been demonstrated. The antenna for the transmitter delivers the power to the receiver with low power loss whereas the coil antenna for the receiver radiates the received power to the bioelectronic system efficiently. The wirelessly received power at the receiver is enough to operate the NFC transponder and the actuation sensors in the actuation system. The actuation system is passivated by soft, flexible, and stretchable materials to allow for mounting on the skin.

The inductive link based on the near-field communication with the bioelectronic application provides the expected power for the operation of bioelectronic devices in the communication distance of 10 ~ 15 cm. However, several improvements to raise the efficiency rate of the radiated power driven to the bioelectronic system are achieved by three main considerations: an impedance matching, a size of the coil, and a number of loops. If the antenna matching at the transmitter is closely matched to 50 Ω, the input return loss is negligible and then no reflected power can occur to minimize the power loss during the wireless power transfer [11], [13]. On the other hand, if the Q factor of the coil antenna for the receiver is close to the maximum Q factor of 20, but does not exceed it, the power received by the receiving coil antenna can be maximized after connecting a shunt capacitor, which provides the resonance at a frequency of 13.56 MHz. Since the antenna inductance depends on the number

of loops and the dimension of the coil antenna, the dimension and number of loops of the coil antenna crucially affect the radiated power to the bioelectronic system. Therefore, the desired power received by the coil antenna can be adjusted [10], [11].

The actuation system consists of seven actuation sensors to generate the vibration and the NFC transponder to manipulate the sensors by the near-field communication data exchange format (NDEF) encoding. Each actuation sensor in the actuation system is activated independent to each other by each of the general-purpose digital input and output terminal (GPIO) signal [20]. In addition, the actuation system is capsulated by the flexible fabric and the layer of PDMS so that the system has flexibility and stretchability to prevent the occurrence of damage. The actuation system also has reusability so that the system can be attached on and off the skin multiple times.

In conclusion, the coil antenna matching circuits can be used in many bioelectronic applications. These antenna designs provide the power with a high-efficiency rate. The coil antennas for wireless power transfer is designed by a cost-effective conductive material, covered by soft, flexible, and stretchable materials, and miniaturized to become portable, especially the receiving coil antenna. Therefore, the coil antennas can be implemented for biomedical studies performed by epidermal electronics with skin-mountable purposes.

# REFERENCES


[1] H. Chung, “A stretchable, soft, and wireless biomedical electronics,” M.S. thesis, University of Illinois at Urbana-Champaign, Urbana, IL, 2016.

[2] D. Kim, N. Lu, R. Ma, Y.-S. Kim, R.-H. Kim, S. Wang, J. Wu, S.M. Won, H. Tao, A. Islam, K.J. Yu, T.-I. Kim, R. Chowdhury, M. Ying, L. Xu, M. Li, H.-J. Chung, H. Keum, M. McCormick, P. Liu, Y.-W. Zhang, F.G. Omenetto, Y. Huang, T. Coleman and J.A. Rogers, “Epidermal electronics,” *Science*, pp. 838-843, 2011.

[3] G. Shin, A.M. Gomez, R. Al-Hasani, Y.R. Jeong, J. Kim, Z. Xie, A. Banks, S.M. Lee, S.Y. Han, C.J. Yoo, J.-L. Lee, S.H. Lee, J. Kurniawan, J. Tureb, Z. Guo, J. Yoon, S.-I. Park, S.Y. Bang, Y. Nam, M.C. Walicki, V.K. Samineni, A.D. Mickle, K. Lee, S.Y. Heo, J.G. McCall, T. Pan, L. Wang, X. Feng, T.-I. Kim, J.K. Kim, Y. Li, Y. Huang, R.W. Gereau IV, J.S. Ha, M.R. Bruchas and J.A. Rogers, "Flexible near-field wireless optoelectronics as subdermal implants for broad applications in Optogenetics," *Neuron,* vol. 93, pp. 509-521, 2017

[4] T.-I. Kim, J.G. McCall, Y.H. Jung, X. Huang, E.R. Siuda, Y. Li, J. Song, Y.M. Song, H.An Pao, R.-H. Kim, C. Lu, S.D. Lee, I.-S. Song, G. Shin, R. Al-Hasani, S. Kim, M.P. Tan, Y. Huang, F.G. Omenetto, J.A. Rogers and M.R. Bruchas, “Injectable, cellular-scale optoelectronics with applications for wireless optogenetics,” *Science,* vol. 240, pp. 211-216, 2013.

[5] Z. Duan, Y.-X. Guo, and D.-L. Kwong, “Rectangular coils optimization for wireless power transmission,” *Radio Science*, vol. 47, no. 3, Jun. 2012.

[6] X. Qing, Z. N. Chen, and M. Y. W. Chia, “Characterization of ultrawideband antennas using transfer functions,” *Radio Science*, vol. 41, no. 1, 2006.

[7] M. Klemm, I. J. Craddock, A. Preece, J. Leendertz, and R. Benjamin, “Evaluation of a hemi-spherical wideband antenna array for breast cancer imaging,” *Radio Science*, vol. 43, no. 6, Dec. 2008.

[8] J. Choi, D. Kang, S. Han, S.B. Kim and J.A. Rogers, "thin, soft, skin-mounted microfluidic networks with capillary bursting valves for Chrono-Sampling of Sweat," *Advanced Healthcare Materials*, vol. 6, no. 5, 2017.

[9] “Why build antennas out of copper and not aluminum or stainless steel,” KB9VBR J-Pole Antennas, 03-Jul-2012. [Online]. Available: http://www.jpole-antenna.com/2012/07/03/why-build-antennas-out-of-copper-and-not-aluminum-or-stainless-steel

[10] S. Magiecrowski, “Small loop antenna calculations,” Fishlab Technical Note, Toronto, ON, Jun. 6, 2007.

[11] “Rectangle Loop Inductance,” Rectangle Loop Inductance | Electronics and Electrical Engineering Tools | EEWeb Community. [Online]. Available: https://www.eeweb.com/toolbox/rectangle-loop-inductance.

[12] V. Todorow, “Impedance matching and matching networks,” *Applied Materials*, 2009.

[13] J. Stiles, “Incident, reflected, and absorbed power,” class notes for EECS 723, Department of Electrical Engineering and Computer Science, University of Kansas, Jan. 27, 2012.

[14] D. M. Pozar, *Microwave Engineering*, 4th ed. Hoboken, NJ: Wiley, pp. 48-94, 2012.

[15] S. J. Franke, *Wireless communication systems*. class notes for ECE 453, Department of Electrical and Computer Engineering, University of Illinois at Urbana-Champaign, pp. 115-133, 2015.

[16] *HF Long Range Reader*, Feig Electronic, Inc., Duluth, GA, 2011.

[17] J. Schillinger, “Antenna matching for the TRF7960 RFID reader,” Texas Instruments, Inc., Dallas, TX, App. Rep. Sep. 2013.

[18] “Ansys Maxwell Calculating the Inductance of WPT Coil,” YouTube, 29-Sep-2014. [Online]. Available: https://www.youtube.com/watch?v=lNWrA-og1NI

[19] “HF Antenna Design Notes,” Texas Instruments, Inc., Dallas, TX, Tech. Rep. 11-08-26-003, Sep. 2003.

[20] *RF430FRL15xH NFC ISO 15693 Sensor Transponder*, Texas Instruments, Inc., Dallas, TX, Dec. 2014.

[21] *74LVC1G384 Bilateral Switch*, Nexperia, B. V., Netherlands, Dec. 2016.

[22] E. Kudeki, “ECE 329 lecture notes on fields & waves," class notes for ECE 329, Department of Electrical and Computer Engineering, University of Illinois at Urbana-Champaign, 2016.

[23] D. B. Hiemstra, G. Parmar, and S. Awtar, “Performance tradeoffs posed by moving magnet actuators in flexure-based nanopositioning,” IEEE/ASME Transactions on Mechatronics, vol. 19, no. 1, pp. 201–212, Feb. 2014.

[24] “What is virtual reality?,” Virtual Reality, 13-Feb-2017. [Online]. Available: https://www.vrs.org.uk/virtual-reality/what-is-virtual-reality.html

[25] J. E. Schutt-Aine, “ADS tutorial on TRL design,” class notes for ECE 451, Department of Electrical Engineering and Computer Engineering, University of Illinois at Urbana-Champaign, Feb. 14, 2017.

[26] *Tutorial 2866: Converting S-Parameters from 50Ω to 75Ω Impedance*, Maxim Integrated, Inc., San Jose, CA, Nov. 21, 2003.

[27] E. Bogatin, "How much return loss is too much?: Rule of thumb #12," EDN, 24-May-2014. [Online]. Available: http://www.edn.com/electronics-blogs/all-aboard-/4430355/How-much-return-loss-is-too-much--Rule-of-Thumb--12